INSTITUTE OF PHYSICS PUBLISHING PLASMA SOURCES SCIENCE AND TECHNOLOGY

Plasma Sources Sci. Technol. **13** (2004) 309–314 PII: S0963-0252(04)78552-7

Spatially resolved emission spectroscopic investigation of microwave-induced reactive low-power plasma jets

Thomas Arnold[1], **Sergey Grabovski**[2], **Axel Schindler**[1] **and Hans-Erich Wagner**[2]

[1] IOM Leipzig, Permoserstr. 15, 04318 Leipzig, Germany
[2] Ernst-Moritz-Arndt-Universität Greifswald, Institut für Physik, Domstraße 10a, 17489 Greifswald, Germany

E-mail: thomas.arnold@iom-leipzig.de

Received 23 May 2003
Published 30 April 2004
Online at stacks.iop.org/PSST/13/309
DOI: 10.1088/0963-0252/13/2/017

Abstract
A microwave-induced Ar/SF_6 plasma jet is characterized by means of optical emission spectroscopy. Rotational temperatures from unresolved N_2 bands and excitation temperatures from Fe lines as well as electron densities (H_β Stark broadening) have been estimated along the plasma jet axis using a side-on configuration. The SF_6 gas flow rate and chamber pressure were varied from 10 to 250 sccm and 20 to 500 mbar, respectively. Three characteristic jet regions have been observed: the plasma ignition zone, followed by the gas mixing zone and a relaxing zone.

1. Introduction

The surface figuring of optical materials (SiO_2, Si, SiC) by means of plasma chemical high-rate etching provides the advantage of preventing the subsurface damages that often occur with mechanical surface figuring techniques. In a previous paper it has been reported that high removal rates can be achieved with a low-power microwave-driven Ar/SF_6/(O_2) plasma jet in a low-pressure regime of about 100 mbar. It has also been shown that for increasing pressure the removal rate decreases [1].

Atmospheric microwave-induced plasma sources have been studied for decades due to their applicability as excitation and ionization sources for atomic spectrometry and mass spectrometry or for remediation of gases and surface treatment. A large variety of microwave plasma sources have been developed and characterized, such as *torche à injection axiale* (TIA) [2], surface wave sustained plasmas [3], microwave cavity plasmas [4], and the microwave plasma torch (MPT) [5]. The plasma source design used for the present investigations is similar to the MPT and TIA, described in [2, 6]. This microwave plasma source produces a stable plasma jet under a wide range of process parameters (ambient pressure (N_2), feed gas flow, gas mixture). On account of the complexity of such a molecular reactive plasma jet, the resulting etching behaviour is not yet completely understood.

In order to characterize the plasma source and to compare it with other plasma sources with similar working principles, spatially resolved optical spectroscopy has been used. Although non-local thermal equilibrium conditions could be expected, processing of spectroscopic data theoretically based on thermal equilibrium has been carried out to compare trends of rotational and excitation temperature as well as electron density. The values obtained in this way will be used in further theoretical investigations as input parameters for a chemical kinetics modelling of the plasma chemistry accompanied by computational fluid dynamics.

2. Experimental set-up

2.1. Plasma source

A schematic diagram of the plasma source is depicted in figure 1(*a*). The source consists of a cross-shaped coaxial wave guide system, which is connected to a coaxial cable supplying a microwave power up to 300 W at 2.45 GHz. On the opposite site of the cable plug a motor-driven short-circuit plunger is attached. One side of the horizontal cross bar is short-circuited, while the other side is open ended. The inner

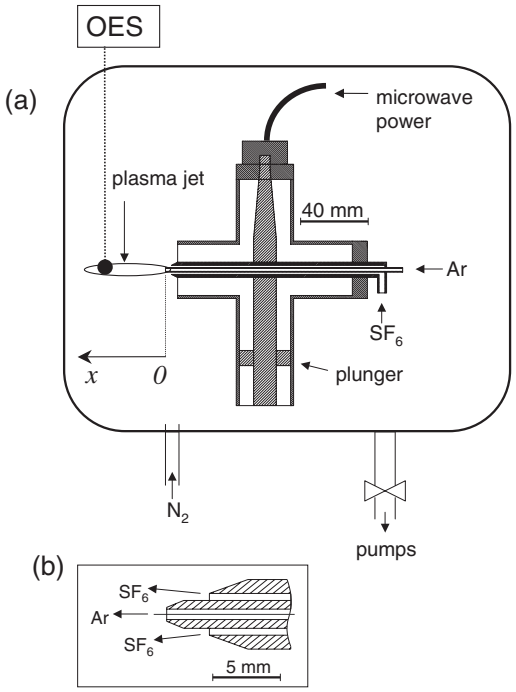

Figure 1. (*a*) Schematic diagram of the microwave plasma torch inside the process chamber. The chamber is not to scale. (*b*) Sketch of the nozzle configuration.

conductor of the horizontal cross bar consists of two coaxial gas feed tubes. At the open end of the inner conductor the plasma jet is created in front of a coaxial nozzle. The inner nozzle diameter is 1.5 mm, and the outer ring-shaped nozzle is 4 mm (inner diameter) and 6 mm (outer diameter) (figure 1(*b*)). The plasma feeding gas flows are controlled by mass flow controllers. The jet is fed by 300 sccm argon as carrier gas through the inner nozzle and 10–200 sccm SF_6 as reactive gas through the outer nozzle. With this configuration it is possible to maintain a stable plasma jet in the technologically relevant pressure regime of 20–300 mbar.

The plasma source is mounted inside a process chamber that can be evacuated by a two-stage rotating-vane/root's pump that allows the ultimate chamber pressure to reach 1 mbar. The ambient pressure is adjusted by N_2 gas let into the process chamber and a closed loop control comprising a Baratron pressure gauge and a butterfly valve in the vacuum line. The ambient pressure was adjusted from 20 to 500 mbar, and the microwave power was set to values between 30 and 300 W.

2.2. Plasma diagnostics and data processing

A Chromex 0.5 m spectrograph with Czerny–Turner configuration and two different selectable gratings (1200 and 300 grooves mm^{-1}) has been used for optical emission measurements. An optical probe connected via a fibre to the spectrograph collects the radiation of the plasma in a side-on configuration with a lateral resolution of about 0.5 mm. The optical probe can be moved in the radial and axial directions relative to the plasma jet manually in stages. For determination of the rotational temperatures, a 300 grooves mm^{-1} grating with an entrance slit width of 80 μm was used. The spectral resolution for this spectrometer configuration was determined

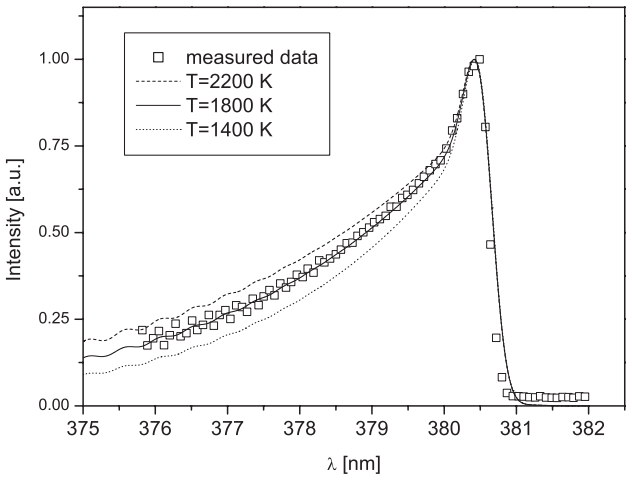

Figure 2. Measured N_2 C–B, 0–2 band and calculated spectra for different rotational temperatures.

to be 0.278 nm from the full-width at half-maximum (FWHM) of the 404.66 nm Hg I line employing an Ar/Hg calibration lamp. The excitation temperatures as well as H_β line widths were determined using the 1200 grooves mm^{-1} grating and an entrance slit width of 80 μm. For this spectrometer configuration a resolution of 0.061 nm (FWHM of 491.60 nm Hg I line) was achieved.

The rotational temperatures have been estimated using the unresolved ($C\,^3\Pi_u$–$B\,^3\Pi_g$; $v' = 0 \rightarrow v'' = 2$) rotational band of nitrogen at 380.5 nm. The measured band shapes were compared with calculated bands, yielding the rotational temperatures from the least-squares fit parameter [7, 8] (figure 2). The estimated error for these measurements is about $\pm$150 K.

Under the assumption that the time of rotational relaxation is much smaller than the mean lifetime of the rotational levels, the rotational distribution is close to a Boltzmann distribution with a temperature, T_{rot}, equal to the kinetic gas temperature [9]. This is assumed to be true for atmospheric pressure plasma jets. Although the lifetime and relaxation time for the spectral transition in the considered gas pressure regime are of the same order of magnitude, and thus the rotational temperatures are expected to be somewhat higher than the gas temperature, the trends of rotational temperatures are comparable with the gas temperatures reported earlier.

Excitation temperatures were measured by sublimating a small amount of ferrocene powder ($C_{10}H_{10}Fe$) into the argon gas [10, 11]. Fe lines in the spectral region around 380 nm were observed. Since several nitrogen bands are present in the spectral region of Fe lines, previously obtained spectra of the same spatial region without ferrocene admixture were subtracted from the Fe line spectra (figure 3(*a*)). Assuming a Boltzmann distribution of the population of the atomic levels, T_{exc} should equal the electron temperature. The emission intensity, I_{ki}, of a transition from level k to level i can be expressed as

$$I_{ki} = C\frac{n g_i f_{ik}}{\lambda_{ki}^3 U(T_{\mathrm{exc}})}\exp\left(-\frac{E_k}{k_{\mathrm{B}}T_{\mathrm{exc}}}\right), \tag{1}$$

$$\ln\left(\frac{I_{ki}\lambda_{ki}^3}{g_i f_{ik}}\right) = -\frac{1}{kT_{\mathrm{exc}}}E_k + \mathrm{const}, \tag{2}$$

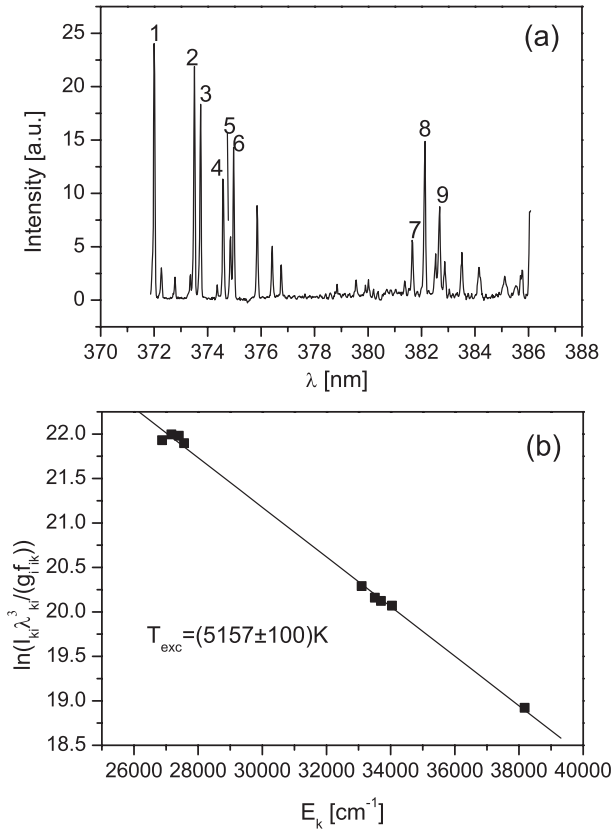

Figure 3. (*a*) Fe line spectrum. (*b*) Boltzmann plot for excitation temperature determination.

Table 1. Spectral data of Fe I lines [12].

No	λ_{ki} (nm)	E_k (cm^{-1})	$g_i f_{ik}$
1	371.99	26 875	0.3698
2	373.49	33 695	2.0749
3	373.71	27 167	0.2679
4	374.56	27 395	0.1694
5	374.82	27 560	0.0964
6	374.95	34 040	1.4488
7	381.58	38 175	1.9861
8	382.04	33 096	1.3152
9	382.59	33 507	0.9183

where g denotes the statistic weight, λ is the wavelength of the transition, f is the oscillator absorption strength, E is the energy, and k is the Boltzmann constant. A Boltzmann plot (equation (2)) was applied to the observed Fe lines listed in table 1.

A linear fit yields the excitation temperature (figure 3(*b*)). The error for excitation temperatures is taken from the standard deviation of the fit. It is of the order of ± 300 K.

As discussed in detail in [13, 14], the atomic state distribution function in microwave-induced plasmas such as MPT and TIA departs from a Boltzmann–Saha equilibrium because of an overpopulation of the lower states. This leads to steeper slopes, $1/(k_B T_{exc})$. Thus the excitation temperature is expected to be smaller than the real electron temperature in the plasma.

Electron densities were estimated through the Stark broadening of the H_β line using the Stark width tables of [15].

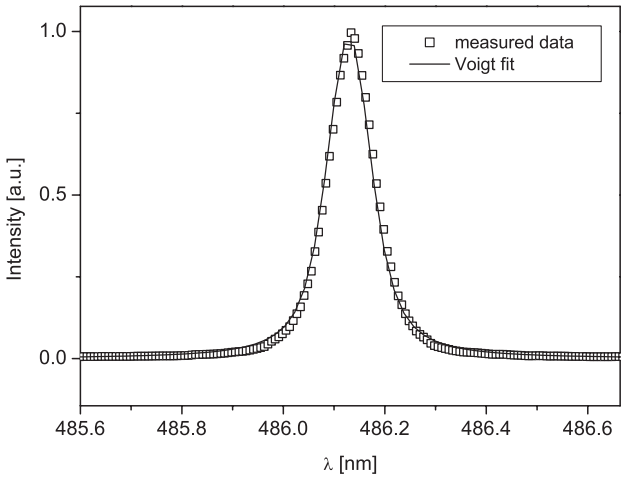

Figure 4. Measured H_β line and Voigt function fit.

For these measurements 1 sccm H_2 was added to the argon gas flow. Due to the convolution of the measured H_β line by the natural line width, Doppler broadening, the response function of the equipment, and Stark broadening, a deconvolution has to be performed. This was done by fitting a Voigt profile with a given Gaussian line width. For a gas temperature of 2300 K the Doppler broadening is 0.019 nm, and the apparatus line profile was determined to be 0.061 nm. Hence, the resulting Gaussian line width of 0.064 nm was removed. As a result, the Lorentzian Stark line width is of the order of $\Delta\lambda_{Stark} = 0.07$ nm. Due to the limited resolution of the spectrometer and imaging errors on the CCD detector, the resulting accuracy of the absolute electron density is about 10% (figure 4).

3. Results and discussion

3.1. Axial profiles

As a result of the coaxial nozzle configuration, a plasma jet is created, with a typical shape as shown in the photograph of figure 5. In order to determine qualitatively the spatial distribution of the species concentrations inside the plasma jet, the emission intensities of three characteristic lines of the gas species involved on the plasma axis was evaluated. Figure 6 shows the axial distribution of the emission line intensities of Ar I (697 nm), F I (686 nm), and N_2 (381 nm). The argon line intensity is constant from the nozzle tip to 6–7 mm above the nozzle and decreases with increasing distance to zero. The fluorine line indicates the presence of atomic fluorine, resulting from the dissociation of SF_6 molecules. The line intensity increases up to 6–8 mm above the nozzle and decreases subsequently. The N_2 intensity increases rapidly for the first 2 mm. It remains constant up to 15 mm and decreases with further distance. From the figures it can be concluded that the concentration of excited species originating from the admixture of SF_6 and N_2 is small at the first 2 mm. Both gases diffuse into the plasma jet. With growing distance from the nozzle, the intermixing gets more and more efficient, probably also due to turbulence at the SF_6/Ar boundary layer.

In figure 7 the rotational and excitation temperatures are shown. The nitrogen rotational temperature is about 800 K

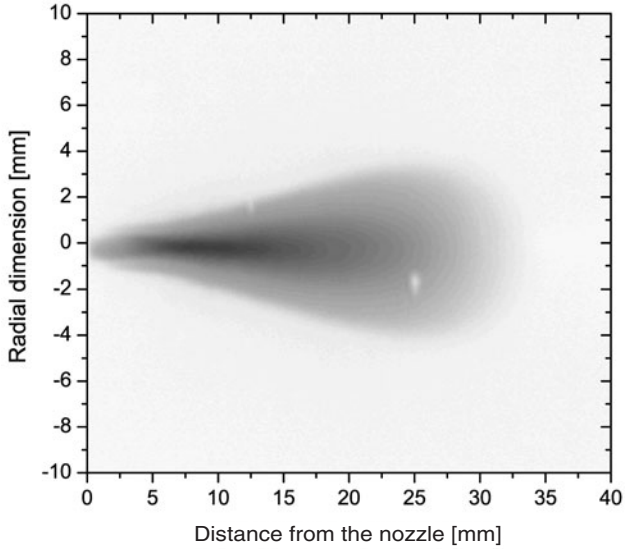

Figure 5. Photograph of a Ar/SF_6 plasma jet at $P = 100$ W, $p = 50$ mbar, [SF_6] = 10 sccm. Dark areas indicate high intensities, white areas stand for low intensities. The photo was taken using a video camera.

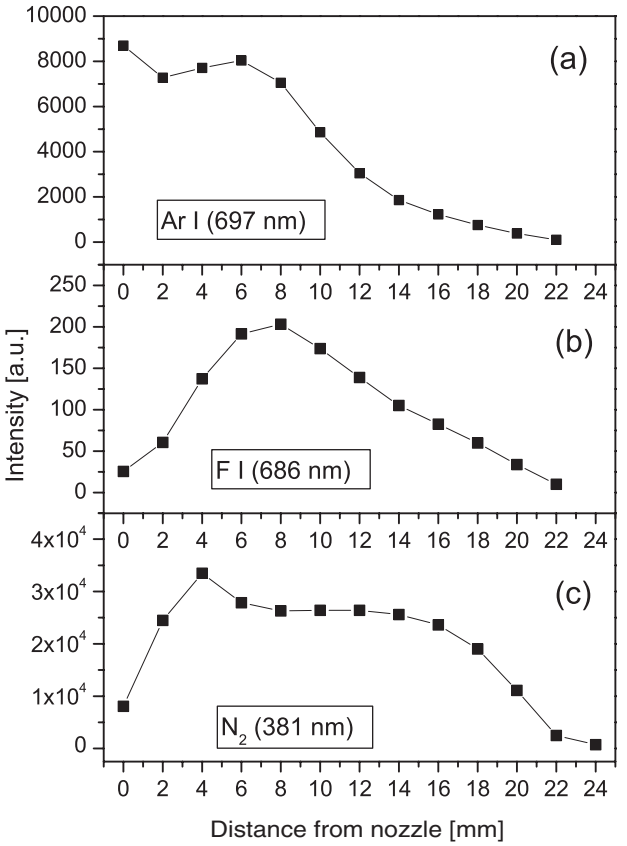

Figure 6. Spatially resolved emission intensities of (*a*) argon line, (*b*) fluorine line, and (*c*) nitrogen band on the plasma jet axis at $P = 60$ W, $p = 50$ mbar, [SF_6] = 50 sccm.

at the nozzle tip, independent of the microwave power. It increases with distance from the nozzle up to a maximum at about 15 mm ($T_{rot} = 2300$ K at $P = 90$ W) and decreases again with larger distances. With increasing power, a faster

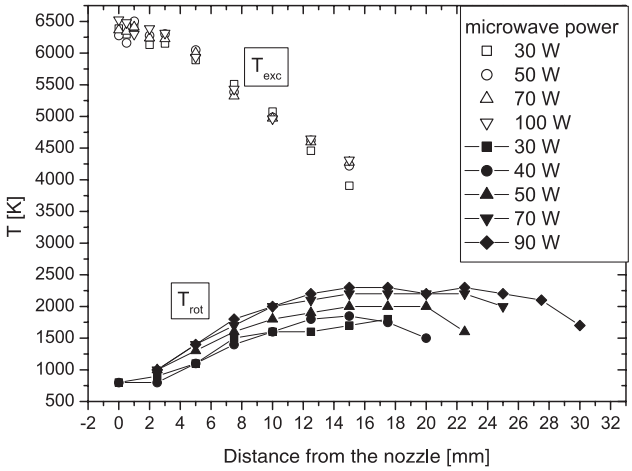

Figure 7. Spatially resolved rotational and Fe excitation temperatures along the plasma jet axis for different microwave input powers.

rise, a higher maximum temperature, and a greater extent of the jet are observed. The trend of an increasing gas temperature with increasing distance from the nozzle is also reported in [16, 17] for the TIA plasma source and in [18] for the MPT, though the absolute maximum temperatures (4500 and 6000 K) are higher.

An explanation for the behaviour of the gas temperature in argon plasma jets is given by Jonkers [17]: molecular nitrogen from the surrounding is entrained by the plasma jet and enters the jet due to diffusion and turbulent gas flow. The processes of ionization of nitrogen molecules via charge transfer,

$$Ar^+ + N_2 \rightarrow Ar + N_2^+, \tag{3}$$

followed by dissociative recombination,

$$N_2^+ + e^- \rightarrow N + N, \tag{4}$$

are loss channels for argon ions and free electrons, respectively. Since the two nitrogen atoms have a relatively high kinetic energy (2 eV), this reaction becomes a significant gas heat source, depending on the radial N_2 flux into the jet.

In the observed plasma, both N_2 and SF_6 gases intrude into the argon jet. In this case at least two other, highly efficient, charge transfer reactions can occur that lead to gas heating [19]:

$$Ar^+ + SF_6 \rightarrow SF_5^+ + Ar + F \tag{5}$$

and [20]

$$N_2^+ + SF_6 \rightarrow SF_5^+ + N_2 + F. \tag{6}$$

This reaction is another loss channel for N_2^+.

The measured Fe excitation temperatures shown in figure 7 are significantly higher than the rotational temperatures. This is characteristic for a non-thermal equilibrium plasma. In the vicinity of the nozzle, the temperature exhibits a value of approximately 6400 K, and from a distance of 2 mm the temperature decreases. At distances larger than 15 mm the absolute Fe emission line intensities were low and covered by strong N_2-related bands in the appropriate spectral region. Thus no temperatures could be measured in this part of the jet.

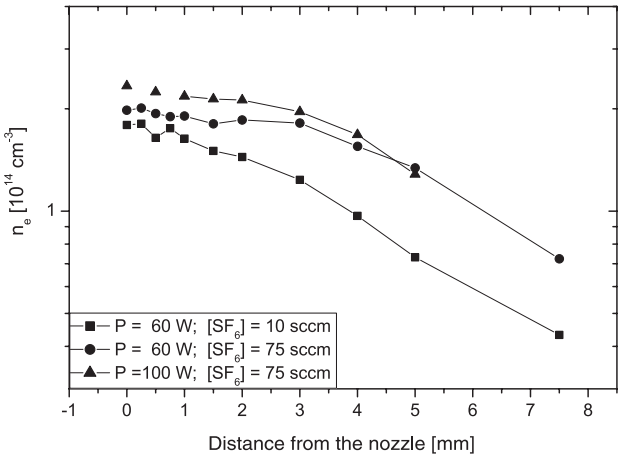

Figure 8. Spatially resolved electron densities along the plasma jet axis for different microwave input powers and SF_6 gas flows, respectively.

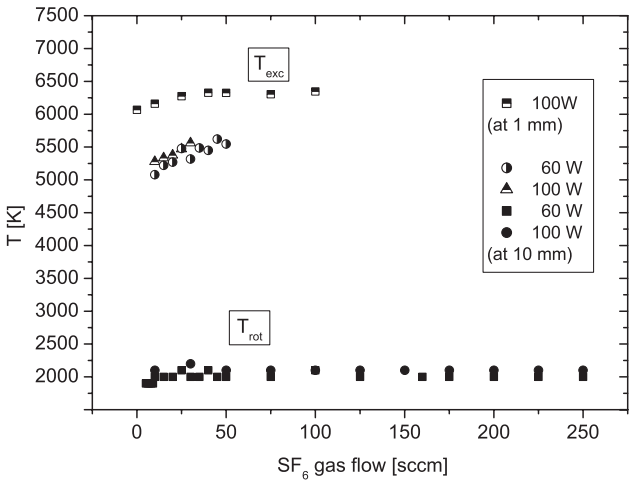

Figure 9. Rotational and Fe excitation temperatures as a function of the SF_6 gas flow. T_{rot} was measured at 15 mm, and T_{exc} was measured at 1 mm and 10 mm distance from the nozzle, respectively.

The reason for the temperature decrease could be an increasing rate of inelastic electron collisions with SF_x, $x = 1, \ldots, 6$, leading to dissociation of the molecule and slower electrons. Within the measurement accuracy no dependence on the applied microwave power has been found. As a comparison, the argon excitation temperatures determined by Jonkers [14] for the TIA are in the range of 4860–8700 K. The electron temperatures that have been measured for the MPT and the TIA by Thomson scattering range from 16 000 to 18 000 K [21, 22].

The axial electron density profile is shown in figure 8. Near the nozzle the electron density shows the highest values. At approximately 2 mm the density starts to decrease. A similar trend is reported in [22] for the TIA atmospheric plasma jet and in [24] for the MPT, but the values are one order of magnitude higher.

In the observed plasma the decrease is probably due to dissociative recombination via equation (4) and formation of SF_x^-, $x = 2, \ldots, 6$ and F^- ions by (dissociative) electron attachment to SF_6, which becomes dominant for electron energies below 0.5 eV [23].

The slightly increased electron densities at higher SF_6 gas flow rates might be explained by a more effective destruction of N_2^+ ions by SF_6, preventing the electron consuming dissociative recombination process.

Comparing the optical emission line distributions in figure 6 and the observed axial temperature profiles, three zones of the plasma jet can be distinguished. The first zone reaches from the nozzle tip to about 2 mm distance. Here a non-thermal argon plasma jet is ignited, forming electrons, positive ions, and metastables. The gas stream is fast but subsonic ($\sim$225 m s^{-1}). As soon as the plasma jet comes into contact with the slow streaming SF_6 or the resting N_2, the jet is slowed down. Concentric diffusion and turbulent mixing from outside into the jet centre occurs. In this region, in the second zone, the admixture of SF_6 and N_2 becomes considerably high. Excitation temperature and electron density decrease as a result of the competing interactions of SF_6 and N_2^+ with electrons. The third plasma zone, starting at about 6–8 mm, is the decay zone. Positive and negative ions and excited species as well as long living atomic and molecular radicals recombine. Stable chemical compounds are formed. The extension of this zone depends on the applied microwave power.

3.2. SF_6 gas flow and ambient pressure

The rotational and excitation temperatures as a function of the SF_6 gas flow are shown in figure 9. Temperatures were determined for two different microwave powers. Rotational temperatures were measured at 15 mm distance from the nozzle (i.e. maximum T_{rot}), the excitation temperatures at 10 mm and 1 mm, respectively, and the electron densities at 1 mm. If a SF_6 flow is present, the rotational temperature is maintained at a constant value. The excitation temperatures as well as the electron density observed at 1 mm above the nozzle also remain constant within the error limits.

Figure 10(*a*) shows the temperatures as a function of the N_2 pressure inside the process chamber. The rotational temperatures obtained for low pressures are generally lower than those measured for TIA or MPT, but they become comparable for higher pressures ($p > 400$ mbar). With increasing ambient pressure the particle density increases and the plasma-forming gas flow velocity decreases. Consequently the diffusion rates become smaller and the residence time of the gas particles in the particular plasma zones rises. This leads to a more effective heating of the gas and a lowering of the excitation temperature because of a higher inelastic collision rate. Also, the electron density at the nozzle tip increases at increasing ambient pressure (as shown in figure 10(*b*)).

4. Conclusion and outlook

Optical emission spectroscopy was applied to a low-power 2.45 GHz microwave-excited Ar/SF_6 plasma jet in which the gases are fed separately in concentric pipes to the nozzle as part of the central conductor of the coaxial wave guide system. Rotational and Fe excitation temperatures as well as electron densities along the jet axis have been spatially resolved, depending on the process parameters SF_6 gas flow and ambient N_2 gas pressure, respectively.

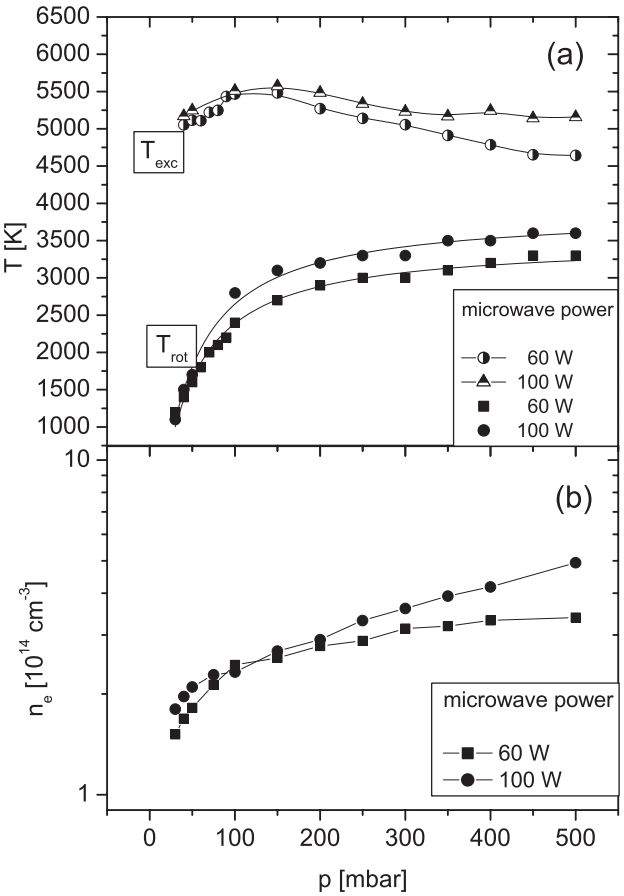

Figure 10. (*a*) Rotational and Fe excitation temperatures measured at 1 mm distance from the nozzle as a function of the N_2 chamber pressure. (*b*) Electron densities measured at 1 mm distance from the nozzle as a function of the N_2 chamber pressure.

In the plasma jet, three different zones can be distinguished. The zone in the vicinity of the gas nozzle is supposed to be the ignition zone, where an argon plasma is created. In the following zone in the direction of the jet the increasing admixture of SF_6 and N_2 into the jet leads to dissociation and excitation of SF_6 and N_2. Dissociative recombination of N_2^+ and inelastic collisions with electronegative species, such as electron (dissociative) attachment, reduce the electron density. Finally, in the third zone, the plasma decays, creating chemically stable compounds. A rising ambient pressure yields a more effective heating of the plasma jet in the decay zone.

It was found that the examined plasma jet shows in general similar trends for the axial temperature distributions and the electron density as in the MPT and the TIA at atmospheric pressure, though the absolute values are higher than in the low-pressure regime.

On the basis of the temperature and density measurements presented in this paper, an existing chemical kinetics model [25] can be extended to a two-dimensional model including fluid dynamics. In order to validate the findings described above and to elucidate the complex interplay between SF_6 and N_2, particle density and flux measurements using a quadrupole mass spectrometer will be carried out.

Acknowledgments

Support for this work from the DFG, FOR 365/2 is gratefully acknowledged.

References

[1] Arnold Th, Boehm G and Schindler A 2001 *J. Vac. Sci. Technol.* A **19** 2586
[2] Moisan M, Sauvé G, Zakrzewski Z and Hubert J 1994 *Plasma Sources Sci. Technol.* **3** 584
[3] Moisan M and Zakrzewski Z 1991 *J. Phys. D: Appl. Phys.* **24** 1024
[4] Beenakker C I M, Bosman B and Boumans P W J M 1978 *Spectrochim. Acta* B **33** 373
[5] Jin Q, Zhu C, Borer M W and Hieftje G M 1991 *Spectrochim. Acta* B **46** 417
[6] Bilgic A M, Prokisch C, Broekaert J A C and Voges E 1998 *Spectrochim. Acta* B **53** 773
[7] Herzberg G 1950 *Molecular Spectra and Molecular Structure* vol 1 (Malabar: Krieger)
[8] Krames B 2000 *PhD Thesis* TU Chemnitz
[9] Phillips D M 1975 *J. Phys. D: Appl. Phys.* **8** 507
[10] Rahman M M and Blades M W 1997 *Spectrochim. Acta* B **52** 1983
[11] Ogura K, Yamada H, Sato Y and Okamoto Y 1997 *Appl. Spectrosc.* **51** 1496
[12] NIST Atomic Spectra Database, http://physics.nist.gov
[13] van der Mullen J A M 1989 *Spectrochim. Acta* B **45** 1
[14] Jonkers J, Vos H P C, van der Mullen J A M and Timmermans E A H 1996 *Spectrochim. Acta* B **51** 457
[15] Gigosos M A and Cardenoso V 1996 *J. Phys.* B **29** 4795
[16] Ricard A, St-Onge L, Malvos H, Gicquel A, Hubert J and Moisan M 1995 *J. Phys. III France* **5** 1269
[17] Jonkers J, Hartgers A, Selen L J, van der Mullen J A M and Schramm D C 1999 *Plasma Sources Sci. Technol.* **8** 49
[18] Huang M, Hanselman D S, Jin Q and Hieftje G M 1990 *Spectrochim. Acta* B **45** 1339
[19] Schwarzer M, Hansel A, Freysinger W, Oberhofer N and Lindinger W 1991 *J. Chem. Phys.* **95** 7344
[20] Richter R, Tosi P and Lindinger W 1987 *J. Chem. Phys.* B **87** 4615
[21] Prokisch C, Bilgic A M, Voges E, Broekaert J A C, Jonkers J, van Sande M and van der Mullen J A M 1999 *Spectrochim. Acta* B **54** 1253
[22] Jonkers J, de Regt J M, van der Mullen J A M, Vos H P C, de Groote F P J and Timmermans E A H 1996 *Spectrochim. Acta* B **51** 1385
[23] Christophorou L G and Olthoff J K 2000 *J. Phys. Chem. Ref. Data* **29** 267
[24] Jovicecic S, Ivkovic M, Pavlovic Z and Konjevic N 2000 *Spectrochim. Acta* B **55** 1879
[25] Arnold Th, Grabovski S, Wagner H-E and Schindler A 2003 *Proc. XXVI ICPIG (Greifswald)* vol 3, p 179